Journal of Power Sources 248 (2014) 337–342

Contents lists available at ScienceDirect

Journal of Power Sources

journal homepage: www.elsevier.com/locate/jpowsour

Hollow spherical carbonized polypyrrole/sulfur composite cathode materials for lithium/sulfur cells with long cycle life

Zhongbao Wang, Shichao Zhang*, Lan Zhang, Ruoxu Lin, Xiaomeng Wu, Hua Fang, Yanbiao Ren

School of Materials Science and Engineering, Beihang University, XueYuan Road No. 37, HaiDian District, Beijing 100191, PR China

HIGHLIGHTS

- Hollow carbonized polypyrrole spheres are prepared by a template method.
- Sulfur is distributed uniformly on the shells of carbonized polypyrrole spheres.
- The carbonized polypyrrole/sulfur composite shows good electrochemical properties.
- The remaining capacity is 758 mA h g^{-1} after 400 cycles at 0.2C rate.

ARTICLE INFO

Article history:
Received 19 June 2013
Received in revised form
4 August 2013
Accepted 21 August 2013
Available online 19 September 2013

Keywords:
Lithium/sulfur battery
Cathode material
Hollow carbonized polypyrrole spheres
Long cycle life

ABSTRACT

Hollow carbonized polypyrrole (PPy) spheres are synthesized using poly(methyl methacrylate–ethyl acrylate–acrylic acid) latex spheres as sacrificial templates. The hollow spherical carbonized PPy/sulfur composite cathode materials are prepared by heating the mixture of hollow carbonized PPy spheres and element sulfur at 155 °C for 24 h. Scanning electron microscope (SEM) and transmission electron microscope (TEM) observations show the hollow structures of the carbonized PPy spheres and the homogeneous distribution of sulfur on the carbonized PPy shells. The hollow spherical carbonized PPy/sulfur composite with 60.9 wt.% S shows high specific capacity and excellent cycling stability when used as the cathode materials in lithium/sulfur cells, whose initial specific discharge capacity reaches as high as 1320 mA h g^{-1} and the reversible discharge capacity retains 758 mA h g^{-1} after 400 cycles at 0.2C. The excellent electrochemical properties benefit from the hollow structures and the flexible shells of the carbonized PPy spheres.

1. Introduction

Rechargeable batteries with high specific energy are highly desired to meet the increasing demands of portable electronic devices, power tools, and electric vehicles [1]. Among the various types of rechargeable batteries, lithium/sulfur (Li/S) battery is a very attractive candidate due to its high theoretical specific capacity of 1675 mA h g^{-1} and high theoretical specific energy of 2600 W h kg^{-1} based on the complete reductions of elemental sulfur with lithium metal to form lithium sulfide (Li_2S). Furthermore, the cathode material sulfur is abundant in various minerals, low cost and environmentally benign [2–6]. Despite these considerable advantages, the application of Li/S batteries still suffers from several serious challenges [7–9], including low utilization of active material sulfur because of its poor electrical conductivity at room temperature and a poor cycle life caused by the dissolution and shuttling effect of the intermediate products lithium polysulfides (Li_2S_n, $4 \leq n < 8$) in organic liquid electrolytes [10–12].

Many efforts have been made to address the challenges described above, including optimization of the organic electrolyte [13], addition of electrolyte additives [14] and combination of a conductive matrix with sulfur to form a highly conductive composite. Conductive matrixes such as mesoporous carbon [15–17], carbon nanotubes [18–20], conductive polymers [21,22] and graphene [23,24] have been investigated to support good conductivity and dispersion of sulfur and also constrain sulfur and the polysulfides within the frameworks. Recent reports suggest that conductive matrixes with hollow structures, such as porous hollow carbon spheres [25], double-shelled hollow carbon spheres [26], polyaniline nanotubes [27] and hollow carbon nanofibers [28] are very promising hosts for sulfur because the hollow carbon structure might have several advantages including high surface area for

* Corresponding author. Tel.: +86 10 82338148; fax: +86 01 82338148.
E-mail address: csc@buaa.edu.cn (S. Zhang).

0378-7753/$ – see front matter © 2013 Elsevier B.V. All rights reserved.
http://dx.doi.org/10.1016/j.jpowsour.2013.08.146

efficient sulfur uptake and polysulfides containment, sufficient space to withstand volumetric expansion and short transport length for Li ions.

In our previous work [29,30], we found that polypyrrole (PPy), with good designable morphology, has high absorption ability to the sulfur and polysulfides within the pore spaces of the polymer matrixes, which can effectively enhance the electrochemical performance of Li/S batteries. In this study, hollow carbonized PPy spheres (HCPSs) were synthesized by in situ chemical oxidative polymerization of pyrrole on the surfaces of monodisperse submicrometer poly(methyl methacrylate–ethyl acrylate–acrylic acid) (PMMA–EA–AA) latex spheres and subsequent pyrolysis of the PMMA–EA–AA templates. The hollow spherical carbonized PPy/sulfur (S/HCPSs) composite prepared by melt-diffusion method exhibited superior cycling stability as cathode for Li/S batteries.

2. Experimental

2.1. Synthesis of PMMA–EA–AA latex spheres

The PMMA–EA–AA latex spheres were prepared by surfactant-free emulsion copolymerization of methyl methacrylate (MMA), ethyl acrylate (EA), and acrylic acid (AA) [31]. At first, 100 ml of deionized water and monomer mixture of 19 ml of MMA, 1 ml of EA and 1.4 ml of AA were added to a four-necked flask immersed in the thermostat water bath in which the temperature was previously adjusted to 80 °C, and stirring speed was controlled at around 300 rpm. Then, 0.29 g of ammonium persulfate (APS) initiator dissolved in 24 ml deionized water was introduced in three steps at different polymerization stages: 16 ml at the beginning, 4 ml at 4 h, and the last 4 ml at 6 h. After 7.5 h of polymerization, the polymerization was continued for an additional 0.5 h at 90 °C.

2.2. Preparation of HCPSs

The HCPSs were prepared by thermal treatment of the PMMA–EA–AA/PPy core–shell composite spheres, which were synthesized by chemical oxidative polymerization using PMMA–EA–AA latex spheres as the cores [32]. Firstly, 2.75 g of $FeCl_3 \cdot 6H_2O$ was solved in 100 ml of the PMMA–EA–AA latex aqueous dispersion (2 wt.% of solid content). Afterward 0.26 ml of PPy was added. After 1 h stirring the polymerization reaction was allowed to continue for about 24 h. The as-prepared black PMMA–EA–AA/PPy composite was separated by filtration and washed with copious amounts of deionized water and then it was dried in a vacuum oven at 60 °C for 24 h.

The thermal treatment was carried out in a tube furnace under N_2 atmosphere. First, the dried PMMA–EA–AA/PPy composite was heated to 350 °C at a heating rate of 4 °C min^{-1}, and the temperature was held at 350 °C for 1.5 h to remove the PMMA–EA–AA templates. Then the temperature was increased to 600 °C at 4 °C min^{-1} and held for 1 h before cooling down to room temperature in order to remove the templates completely.

2.3. Preparation of S/HCPSs composite cathode materials

The S/HCPSs composite was prepared as the follows: the mixture of HCPSs and sulfur was mixed with weight ratio of 4:7 and sealed in a polytetrafluoroethylene (PTFE) container filled with argon gas. Then the container was placed in an oven at 155 °C for 24 h before cooling down to room temperature.

2.4. Material characterization

Fourier-transform infrared (FTIR) spectra were recorded using a Nicolet 6700 spectrophotometer. The morphology of the samples was investigated by a Hitachi S-4800 scanning electron microscope (SEM) and a JEM-2100F transmission electron microscope (TEM). Raman spectra were carried out on a Renishew-1000 system with a He–Ne lamp-house. Thermogravimetric analysis (TGA) was performed on a NETZSCH STA 449C thermal analyzer under N_2 atmosphere at a heating rate of 10 °C min^{-1}. The crystalline status was characterized by a Rigaku X-ray diffraction (XRD) using Cu Kα radiation. The specific surface area was measured with Brunauer–Emmett–Teller (BET) measurement with N_2.

2.5. Electrochemical measurements

The composite cathode slurry was made by mixing 70% S/HCPSs composite, 20% carbon black and 10% polyvinylidene fluoride (PVDF) binder in *N*-methyl-2-pyrrolidinone (NMP) solvent. After homogeneous mixing, the slurry was uniformly coated onto aluminum foil substrates. The coated electrodes were dried in a vacuum oven at 50 °C for 24 h and cut to an 8 mm × 8 mm size subsequently. The HCPSs cathode with 70% HCPSs, 20% carbon black and 10% PVDF binder was prepared in the same way for comparison. CR 2032 coin-type cells were assembled in an Ar-filled glove box (Mbraun, Unilab, Germany), with Celgard 2300 membrane as separator, Li foil as counter electrode and 1 M $LiCF_3SO_3$ in a mixed solution of DOL and DME (1:1 in volume ratio) as electrolyte. The cells were galvanostatically discharged and charged on a Neware BTS-610 battery test system in a voltage range of 1.5–3.0 V (vs. Li/Li^+) at different current densities. Cyclic voltammetry (CV) measurements were performed on a CHI660D electrochemical workstation at a scanning rate of 0.1 mV s^{-1} between 1.5 and 3.0 V (vs. Li/Li^+).

3. Results and discussion

FTIR spectra of PMMA–EA–AA latex spheres, PMMA–EA–AA/PPy core–shell composite spheres and HCPSs are shown in Fig. 1. The two strongest characteristic absorption peaks of PMMA–EA–AA at 1732 and 1151 cm^{-1} are ascribed to the stretching vibration of the C=O bond and the C–O bond respectively [33,34]. The FTIR spectrum of PMMA–EA–AA/PPy composite spheres includes both the characteristic peaks of PMMA–EA–AA at 1732 and 1183 cm^{-1}

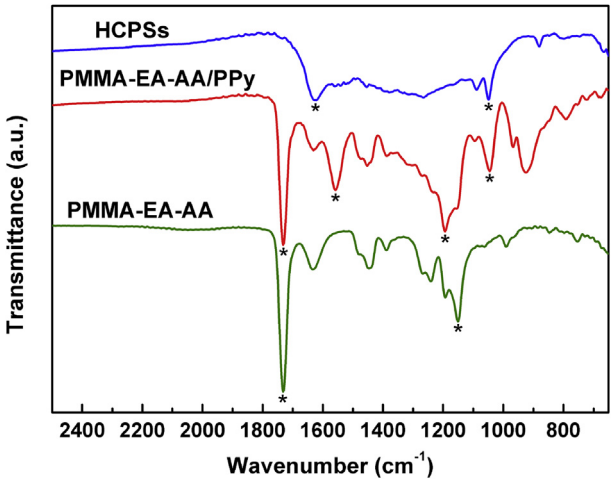

Fig. 1. FTIR spectra of PMMA–EA–AA spheres, PMMA–EA–AA/PPy spheres and HCPSs.

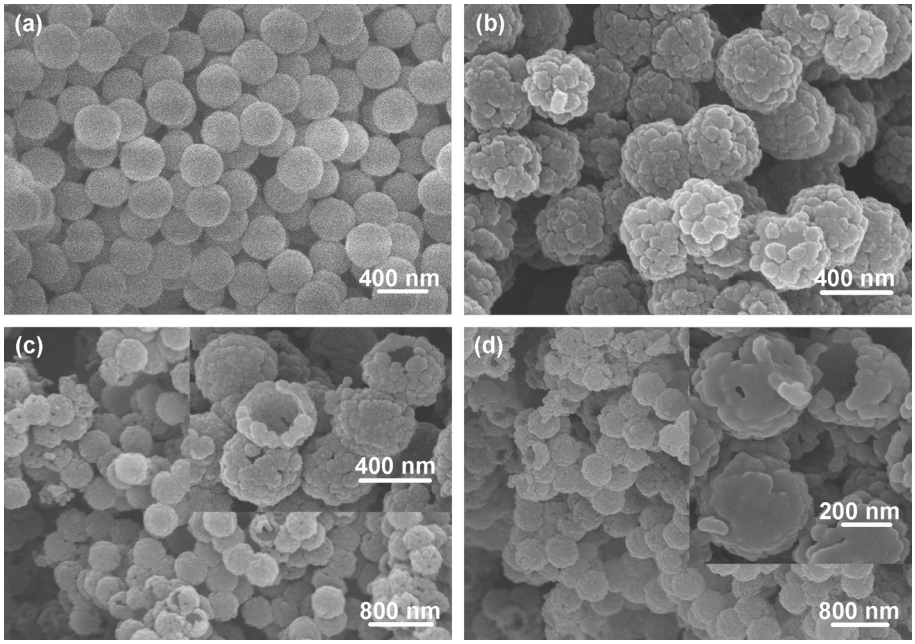

Fig. 2. SEM images of (a) PMMA–EA–AA spheres, (b) PMMA–EA–AA/PPy spheres, (c) HCPSs with an inset at higher magnification and (d) S/HCPSs composite with an inset at higher magnification.

and the characteristic peaks of PPy at 1558 and 1045 cm^{-1} corresponding to the pyrrole rings vibration and the =C–H in-plane vibration [30,35]. In the FTIR spectrum of HCPSs, the characteristic peaks at 1620 and 1049 cm^{-1} can be ascribed to the pyrrole ring fundamental vibration and =C–H in plane bending of PPy [30,33]. The characteristic peaks of PPy become weaker due to the carbonation of HCPSs and no characteristic peaks of PMMA–EA–AA are found which suggests that the PMMA–EA–AA templates have been completely removed by the thermal treatment.

Fig. 2 shows the SEM morphological characterization of PMMA–EA–AA latex spheres, PMMA–EA–AA/PPy composite spheres, HCPSs and S/HCPSs composite. Fig. 3 shows the TEM images of HCPSs and S/HCPSs composite. As seen, the average diameter of HCPSs is approximately 450 nm and the shell thickness is about 80 nm. It can be seen from Fig. 2a and b that PPy grows in irregularly distributed nodules on the surfaces of the PMMA–EA–AA spheres and PPy coatings present some fissures and pores between the nodules. After pyrolysis of the templates, the fissures and pores

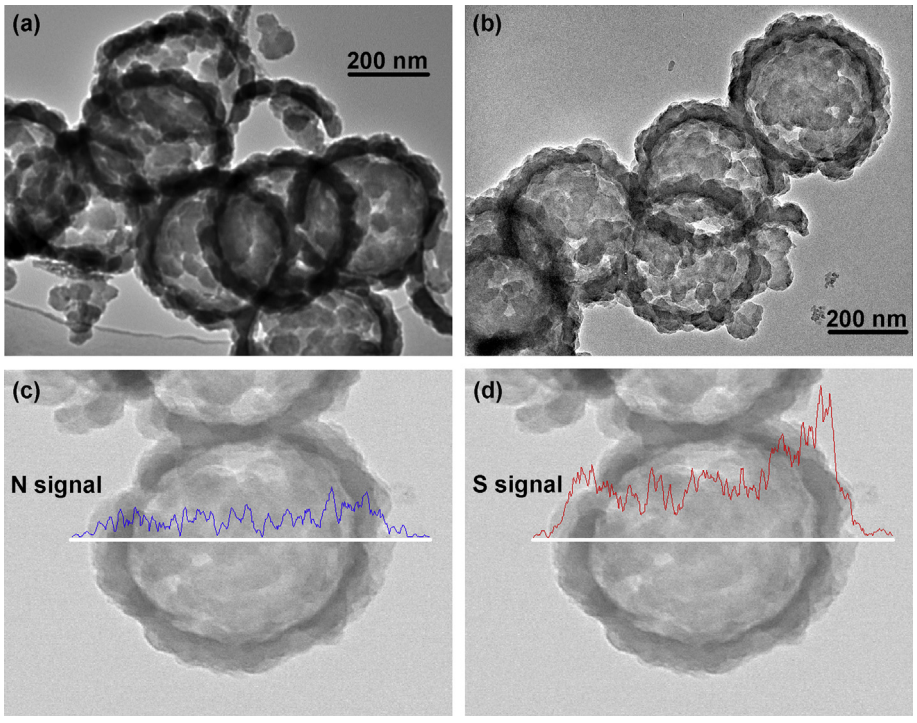

Fig. 3. TEM images of (a) HCPSs, (b) S/HCPSs composite and (c, d) EDS line scanning of S/HCPSs composite.

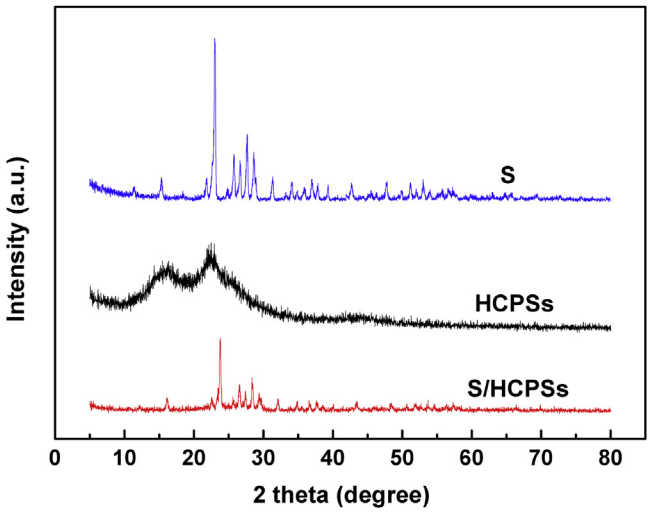

Fig. 4. XRD patterns of sulfur, HCPSs and S/HCPSs composite.

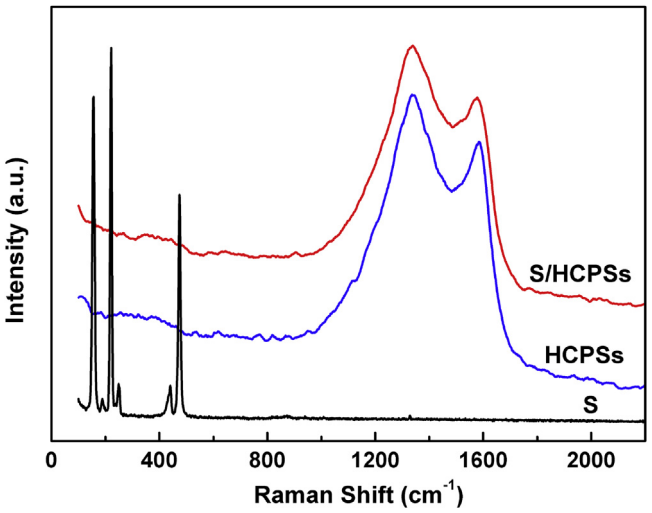

Fig. 6. Raman spectra of sulfur, HCPSs and S/HCPSs composite.

remain on the shells of the HCPSs as shown in Figs. 2c and 3a. Some of the HCPSs rupture due to incomplete PPy coatings on the templates or the pressure of small-molecule gases produced during the pyrolysis of the templates. The HCPSs sample shows a high BET specific surface area of 106 $m^2\ g^{-1}$ and a large total pore volume of 0.577 $cm^3\ g^{-1}$. The soft shells with high specific surface area can effectively constrain the sulfur and polysulfides within the pore spaces of the carbonized PPy matrixes. The holes and fissures on the shells are beneficial for the penetration of melting sulfur and

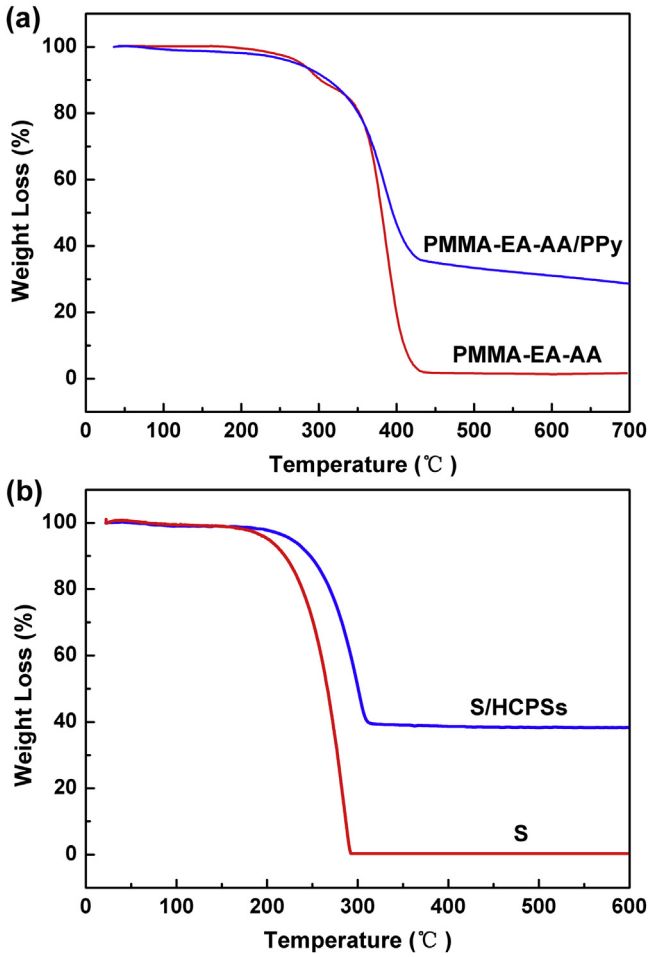

Fig. 5. (a) TGA curves of PMMA–EA–AA spheres and PMMA–EA–AA/PPy spheres. (b) TGA curves of sulfur and S/HCPSs composite.

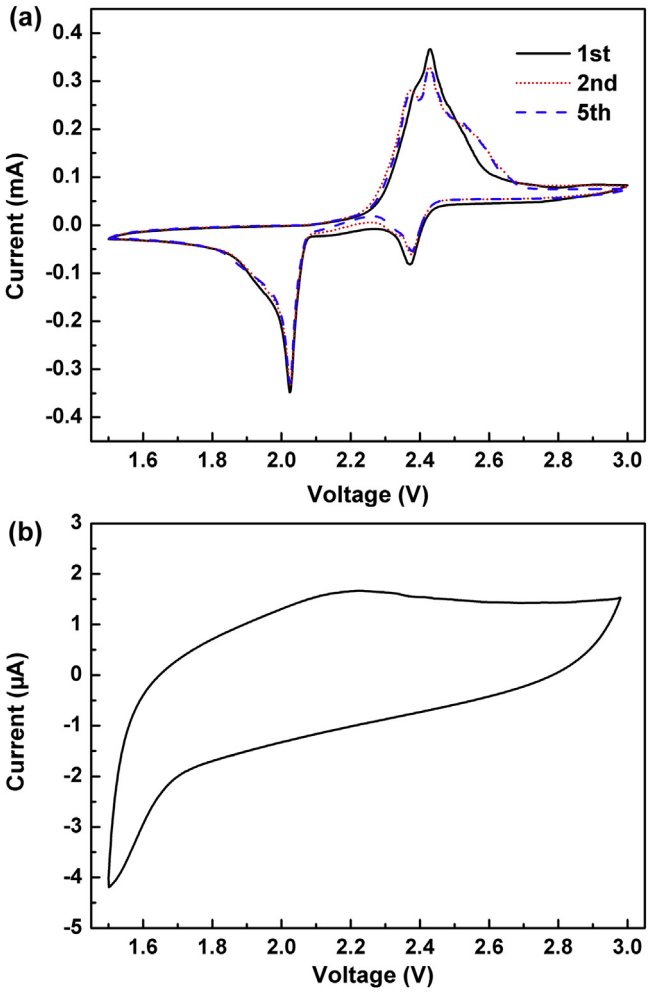

Fig. 7. CV curves of (a) S/HCPSs composite electrode and (b) HCPSs electrode at 0.1 mV s^{-1}.

electrolyte into the HCPSs, so the polysulfides dissolved in electrolyte could be restricted within the HCPSs. The SEM and TEM images of S/HCPSs composite in Figs. 2d and 3b show similar morphology compared to the pristine HCPSs and no discernible sulfur particles are found inside or outside the hollow spheres, which suggests the homogeneous distribution of sulfur on the carbonized PPy shells. The energy-dispersive X-ray spectroscopy (EDS) spectra of the S/HCPSs composite as seen in Fig. 3c and d prove the existence of nitrogen and sulfur in the composite, and the consistent signals indicate the distribution of the sulfur is uniform.

The XRD patterns of elemental sulfur, HCPSs and S/HCPSs composite are shown in Fig. 4. The reflections of the elemental sulfur are consistent with Fddd orthorhombic structure [30]. The XRD pattern of HCPSs shows a typical amorphous structure with two broad low-intensity peaks, which are attributed to the periodicity parallel and perpendicular to the carbonized PPy chains [27]. For the S/HCPSs composite, the peaks with much reduced intensity compared with that of elemental sulfur indicate good dispersion of sulfur on the carbonized PPy shells [36], which is in good agreement with the above SEM and TEM images.

Fig. 5 presents the TGA curves of PMMA–EA–AA latex spheres, PMMA–EA–AA/PPy composite spheres, sulfur and S/HCPSs composite. TGA curves of PMMA–EA–AA spheres and PMMA–EA–AA/PPy spheres as seen in Fig. 5a indicate the decomposition of the core PMMA–EA–AA spheres starts at 300 °C. Most of the PMMA–EA–AA spheres have decomposed and disappeared by 440 °C. The weight loss between 440 °C and 700 °C is mainly caused by the decomposition of the PPy shells to form various N-containing byproducts such as HCN and N_2 [37]. TGA of the S/HCPSs composite as seen in Fig. 5b shows a weight loss of 60.9% from 150 °C to over 300 °C and the reduction in weight is due to the evaporation of sulfur [26]. Hence the sulfur content is 60.9 wt.% in the S/HCPSs composite. The sulfur in the composite exhibits a better thermal stability compared with pure elemental sulfur, which indicates the strong interaction between the sulfur and carbonized PPy [38].

Fig. 6 shows the Raman spectra of elemental sulfur, HCPSs and S/HCPSs composite. The Raman spectrum of the HCPSs contains two strong peaks at 1350 and 1580 cm^{-1}, which are identified as the characteristic peaks of C–N and C–C groups respectively [30]. No new peaks are found in the spectrum of the S/HCPSs composite compared with that of the HCPSs, indicating good dispersion of sulfur and no chemical reaction between sulfur and carbonized PPy happened during the co-heating process.

The CV curves of S/HCPSs composite and HCPSs are shown in Fig. 7. As seen in Fig. 7a, the CV curves of S/HCPSs composite show two reduction peaks at around 2.4 and 2.0 V. The first peak at 2.4 V corresponds to the transformation of elemental sulfur to long-chain soluble lithium polysulfides (Li_2S_n, $4 \leq n < 8$) and the second peak at 2.0 V involves the reduction of the lithium polysulfides to insoluble Li_2S_2 and Li_2S [21]. The oxidation peaks are at around 2.45 V. No obvious changes are observed in the peak currents and potentials after 5 scans, indicating good reactive reversibility and structural stability of the composite electrode [25]. The CV curve of HCPSs presented in Fig. 7b shows no distinctive reduction and oxidation peaks between 1.5 and 3.0 V (vs. Li/Li^+), so the electrochemical activity of HCPSs can be neglected in the S/HCPSs composite electrode.

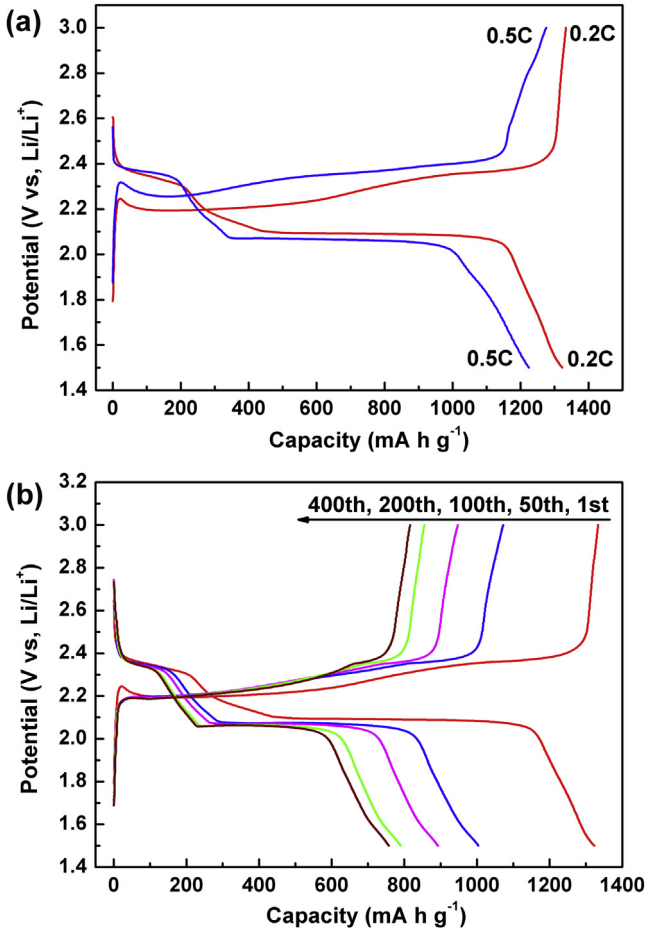

Fig. 8. (a) Initial discharge/charge voltage profiles of the S/HCPSs composite electrode at 0.2C and 0.5C. (b) Typical discharge/charge voltage profiles of the electrode at 0.2C.

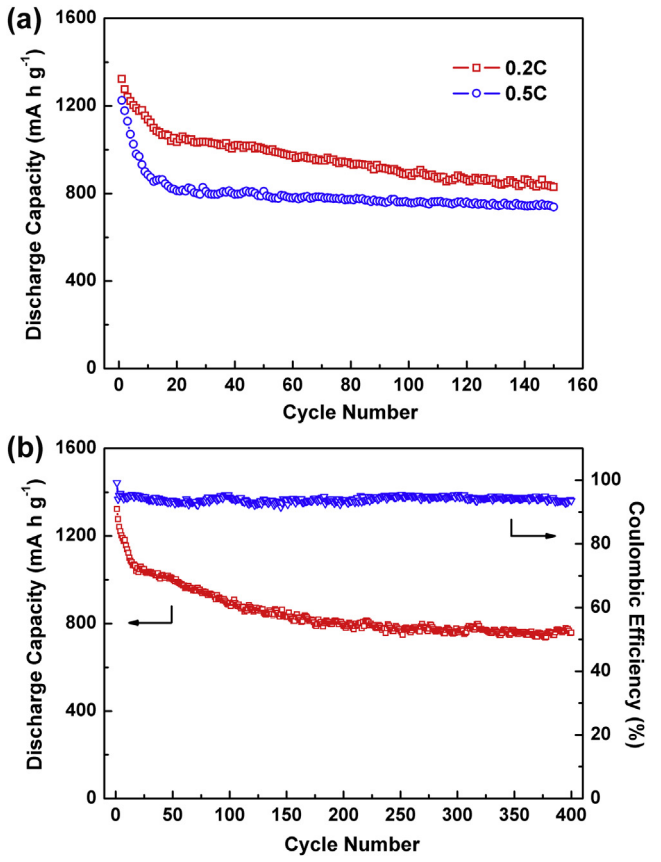

Fig. 9. (a) Cycling performance of the S/HCPSs composite electrode at 0.2C and 0.5C. (b) Prolonged cycling performance and coulombic efficiency of the electrode up to 400 cycles at 0.2C.

Fig. 8 shows the discharge/charge voltage profiles of the S/HCPSs composite. The initial discharge curves at both 0.2C and 0.5C (by weight of sulfur, 1C = 1675 mA g^{-1}) as seen in Fig. 8a show the typical two-plateau behavior of a Li/S cell, which is due to the two step reaction of S with Li during the discharge process as demonstrated in CV measurement. As shown in Fig. 8b, the S/HCPSs composite shows a good utilization of active material with an initial specific discharge capacity of 1320 mA h g^{-1} and maintains a reversible capacity of 758 mA h g^{-1} after 400 cycles at a rate of 0.2C. In addition, all the discharge curves show two distinct plateaus, confirming the stable existence of elemental sulfur and polysulfides in the pore spaces within the carbonized PPy matrixes even after 400 cycles [39]. These indicate that the HCPSs are quite effective in suppressing the dissolution of polysulfides into the electrolyte and in maintaining high utilization of the active sulfur during the discharge/charge process.

The cycling performance of the S/HCPSs composite is presented in Fig. 9. As seen in Fig. 9a, the composite shows an initial specific discharge capacity of 1320 mA h g^{-1} with a reversible capacity of 830 mA h g^{-1} retained after 150 cycles at 0.2C rate. Within the initial 20 cycles the discharge capacity decreases quickly to 1035 mA h g^{-1}, and then becomes relatively stable. From the 20th to the 150th cycle, the capacity only decreases by 19.8%. The quick capacity decay in the initial stage is likely due to the superficial sulfur deposited on the surfaces of the HCPSs. The stable capacity after 20 cycles shows good cycling stability of the S/HCPSs composite. At a higher rate of 0.5C, an initial capacity of 1225 mA h g^{-1} is measured and the capacity retains 739 mA h g^{-1} after 150 cycles. After 20 cycles, the capacity decreases to 812 mA h g^{-1} and becomes more stable (9% of decay from the 20th to the 150th cycle) than at the rate of 0.2C, which is likely due to less shuttle effect at higher current density [23] after the quick capacity decay in the initial stage. At the 0.2C rate, the more stable capacity is also found after 200 cycles as seen in Fig. 9b. The capacity decreases to 790 mA h g^{-1} after 200 cycles and then becomes more stable (4% of decay from the 200th to the 400th cycle). Besides, the coulombic efficiency at 0.2C rate shown in Fig. 9b is averagely at 94% except the first cycle (99.2%).

The high specific capacity and excellent cycling stability of the S/HCPSs composite can probably be attributed to the hollow structures of the carbonized PPy spheres with some holes and fissures on the shells. The electrolyte can penetrate into the shells and interior void spaces of HCPSs through the holes and fissures, which greatly increases the transport rate of Li ions to the sulfur. When migrating outward, the dissolved polysulfides in the interior void spaces can be reabsorbed by the carbonized PPy shells during the repeated discharge/charge of the electrode. This may explain the stable capacity after initial decay due to the superficial sulfur. Meanwhile, the soft carbonized PPy shells could provide strong physical confinement to the element sulfur and polysulfides and accommodate the volume change associated with the electrochemical reactions.

4. Conclusions

HCPSs were synthesized by a template method and the S/HCPSs composite cathode materials were prepared via a simple co-heating technique. The composite cathode materials exhibited good electrochemical properties in rechargeable Li/S cells. The initial specific discharge capacity was up to 1320 mA h g^{-1} and the remaining capacity was 758 mA h g^{-1} even after 400 cycles at a rate of 0.2C. We attribute the excellent cycling stability of the S/HCPSs composite to the hollow structures of the HCPSs and the flexible carbonized PPy shells which can effectively constrain the sulfur and polysulfides.

Acknowledgments

This work was supported by National High Technology Research and Development Program of China (2011AA11A257), National Basic Research Program of China (2013CB934001) and National Natural Science Foundation of China (50954005 and 51074011).

References

[1] J. Wang, J. Chen, K. Konstantinov, L. Zhao, S.H. Ng, G.X. Wang, Z.P. Guo, H.K. Liu, Electrochim. Acta 51 (2006) 4634–4638.
[2] J. Sun, Y. Huang, W. Wang, Z. Yu, A. Wang, K. Yuan, Electrochem. Commun. 10 (2008) 930–933.
[3] L. Ji, M. Rao, S. Aloni, L. Wang, E.J. Cairns, Y. Zhang, Energy Environ. Sci. 4 (2011) 5053–5059.
[4] H. Kim, J.T. Lee, G. Yushin, J. Power Sources 226 (2013) 256–265.
[5] G.C. Li, G.R. Li, S.H. Ye, X.P. Gao, Adv. Energy Mater. 2 (2012) 1238–1245.
[6] Y. Yang, G. Zheng, S. Misra, J. Nelson, M.F. Toney, Y. Cui, J. Am. Chem. Soc. 134 (2012) 15387–15394.
[7] X. Liang, Y. Liu, Z. Wen, L. Huang, X. Wang, H. Zhang, J. Power Sources 196 (2011) 6951–6955.
[8] F. Wu, J. Chen, L. Li, T. Zhao, R. Chen, J. Phys. Chem. C 115 (2011) 24411–24417.
[9] W. Wei, J. Wang, L. Zhou, J. Yang, B. Schumann, Y. NuLi, Electrochem. Commun. 13 (2011) 399–402.
[10] G. He, X. Ji, L. Nazar, Energy Environ. Sci. 4 (2011) 2878–2883.
[11] Y.S. Su, A. Manthiram, Electrochim. Acta 77 (2012) 272–278.
[12] W. Ahn, K.B. Kim, K.N. Jung, K.H. Shin, C.S. Jin, J. Power Sources 202 (2012) 394–399.
[13] J. Gao, M.A. Lowe, Y. Kiya, H.D. Abruna, J. Phys. Chem. C 115 (2011) 25132–25137.
[14] X. Liang, Z. Wen, Y. Liu, M. Wu, J. Jin, H. Zhang, X. Wu, J. Power Sources 196 (2011) 9839–9843.
[15] C. Liang, N.J. Dudney, J.Y. Howe, Chem. Mater. 21 (2009) 4724–4730.
[16] X. Li, Y. Cao, W. Qi, L.V. Saraf, J. Xiao, Z. Nie, J. Mietek, J.G. Zhang, B. Schwenzer, J. Liu, J. Mater. Chem. 21 (2011) 16603–16610.
[17] S.R. Chen, Y.P. Zhai, G.L. Xu, Y.X. Jiang, D.Y. Zhao, J.T. Li, L. Huang, S.G. Suna, Electrochim. Acta 56 (2011) 9549–9555.
[18] J. Guo, Y. Xu, C. Wang, Nano Lett. 11 (2011) 4288–4294.
[19] L. Yuan, H. Yuan, X. Qiu, L. Chen, W. Zhu, J. Power Sources 189 (2009) 1141–1146.
[20] J. Chen, X. Jia, Q. She, C. Wang, Q. Zhang, M. Zheng, Q. Dong, Electrochim. Acta 55 (2010) 8062–8066.
[21] F. Wu, J. Chen, R. Chen, S. Wu, L. Li, S. Chen, T. Zhao, J. Phys. Chem. C 115 (2011) 6057–6063.
[22] L. Wang, X. He, J. Li, M. Chen, J. Gao, C. Jiang, Electrochim. Acta 72 (2012) 114–119.
[23] H. Wang, Y. Yang, Y. Liang, J.T. Robinson, Y. Li, A. Jackson, Y. Cui, H. Dai, Nano Lett. 11 (2011) 2644–2647.
[24] J.Z. Wang, L. Lu, M. Choucair, J.A. Stride, X. Xu, H.K. Liu, J. Power Sources 196 (2011) 7030–7034.
[25] N. Jayaprakash, J. Shen, S.S. Moganty, A. Corona, L.A. Archer, Angew. Chem. Int. Ed. 50 (2011) 5904–5908.
[26] C. Zhang, H.B. Wu, C. Yuan, Z. Guo, X.W. Lou, Angew. Chem. Int. Ed. 51 (2012) 1–5.
[27] L. Xiao, Y. Cao, J. Xiao, B. Schwenzer, M.H. Engelhard, L.V. Saraf, Z. Nie, G.J. Exarhos, J. Liu, Adv. Mater. 24 (2012) 1176–1181.
[28] G. Zheng, Y. Yang, J.J. Cha, S.S. Hong, Y. Cui, Nano Lett. 11 (2011) 4462–4467.
[29] M. Sun, S. Zhang, T. Jiang, L. Zhang, J. Yu, Electrochem. Commun. 10 (2008) 1819–1822.
[30] L. Qiu, S. Zhang, L. Zhang, M. Sun, W. Wang, Electrochim. Acta 55 (2010) 4632–4636.
[31] K. Kang, C.Y. Kan, Y. Du, D.S. Liu, J. Appl. Polym. Sci. 92 (2004) 433–438.
[32] M.I. Redondo, M.V. García, E. Sánchez de la Blanca, M. Pablos, I. Carrillo, M.J. González-Tejera, E. Enciso, Polymer 51 (2010) 1728–1736.
[33] H. Chen, W. Wang, G. Li, C. Li, Y. Zhang, Synth. Met 161 (2011) 1921–1927.
[34] D.B. Cairns, M.A. Khan, C. Perruchot, A. Riede, S.P. Armes, Chem. Mater. 15 (2003) 233–239.
[35] H. Zhang, X. Zhong, J.J. Xu, H.Y. Chen, Langmuir 24 (2008) 13748–13752.
[36] W. Zhang, D. Qiao, J. Pan, Y. Cao, H. Yang, X. Ai, Electrochim. Acta 87 (2013) 497–502.
[37] H. Dong, W.E. Jones Jr., Langmuir 22 (2006) 11384–11387.
[38] M.Q. Zhao, X.F. Liu, Q. Zhang, G.L. Tian, J.Q. Huang, W. Zhu, F. Wei, ACS Nano 6 (2012) 10759–10769.
[39] M. Rao, W. Li, E.J. Cairns, Electrochem. Commun. 17 (2012) 1–5.